

Dynamic Electrostatic Lithography: Multiscale On-Demand Patterning on Large-Area Curved Surfaces

Qiming Wang, Mukarram Tahir, Jianfeng Zang, and Xuanhe Zhao*

Using electrical voltages to form self-organized patterns on polymer surfaces has been intensively studied for a diverse range of scientific and technological applications including functional surfaces and interfaces,^[1] integrated electronics,^[2] optoelectronics,^[3] data storage,^[4] sensor arrays,^[4,5] microfluidics^[6] and biomedical devices.^[7] The technology so-called *electrostatic lithography* is generally based on a mask-air-polymer system,^[2] where a voltage is applied from a top electrode (i.e. mask) through an air gap to one or multiple layers of polymer melts bonded on a bottom electrode (see Figure S1). Despite the intensive studies and broad applications of *electrostatic lithography*,^[2,5,8] the technology suffers from a number of limitations: (1) the patterns formed with this method are generally static in that only the final patterns are solidified for uses. Therefore, the polymer surfaces cannot dynamically switch among multiple states (e.g. patterned and flat) in practical applications. (2) The requirement for precise alignment of the top mask, air gap, and polymer limits this method to relatively small-area and flat surfaces.^[9] (3) The relatively low breakdown field of the air gaps^[10] (i.e., $\sim 10^6$ V/m) mandates the use of polymer melts or very soft elastomers (e.g. modulus ~ 1 kPa).^[10] (4) This method generally gives convex patterns (e.g. pillars) on polymer surfaces,^[2] but not concave patterns (e.g. trenches, creases and holes et al) which are equally, if not more, desirable features.^[11] These limitations greatly hamper the tunability and flexibility of *electrostatic lithography*, restraining its application in various important technologies such as on-demand super-hydrophobicity,^[12] tunable adhesion,^[13] switchable optics,^[14] controlled drug release,^[15] anti-fouling coatings,^[16] and transfer printing.^[17]

Here, we present a new method and material system capable of dynamically generating a rich variety of patterns on large-area curved polymer surfaces using electric fields up to 10^8 V/m. Because the most distinct feature of the new method is its capability of dynamic patterning, we name the new method as *dynamic electrostatic lithography* (DEL). The DEL can switch polymer surfaces among various patterns ranging from randomly-oriented creases and craters to aligned creases, craters and lines (see Figure 1C, Video S1 and Video S2). The length scale of the

patterns is controllable, ranging from millimeter to micrometer (Figure 1D). In addition, the patterning with DEL is generally much faster than that with stimuli-responsive hydrogels,^[11,18] shape-memory polymers,^[19] and swellable polymers.^[20,21] Furthermore, electric voltages can also be more precisely controlled than other stimuli including mechanical contact,^[22] temperature,^[11,19] pH^[18], solvent concentration^[21] and humidity.^[23]

The material system for DEL is illustrated in Figure 1A (see the Experimental Section for details). A layer of a solid polymer is bonded on an insulating substrate. The modulus of the polymer can reach 10 MPa, much higher than the moduli allowed in traditional *electrostatic lithography*. The polymer layer can also be uniaxially pre-stretched prior to bonding on the substrate. The insulating substrate is chosen to be much more rigid than the polymer, so that it does not deform with the polymer during patterning.^[24,25] The bottom surface of the substrate is coated with a metal layer (e.g. gold), and the top surface of the polymer is covered with a compliant electrode (e.g. NaCl solution,^[24,25] liquid metal,^[26] nanowire^[27] or carbon nanotube^[28] electrodes), which deforms conformally with the polymer surface. Because the DEL eliminates the requirement for mask-air-polymer alignment, the polymer layers in DEL can be easily fabricated into very large areas and cover curved surfaces as well.

The mechanism of the DEL is qualitatively understood as follow. The dynamic patterns of DEL are caused by electro-mechanical instabilities of polymer layers under electric fields recently discovered.^[24,29] As a direct-current voltage is applied between the two electrodes, an electric field develops in the polymer layer. The electric field induces a biaxial compressive stress σ_E in the polymer layer. When the electric field reaches a critical value, the initially flat polymer surface suddenly folds against itself, forming a pattern of randomly-oriented creases on the polymer^[24] (Figure 1C). As the electric field further increases, the electric-field-induced stress tends to pull the creases open into randomly-oriented craters in the polymer layer^[24] (Figure 1C). If the polymer layer has been uniaxially pre-stretched as illustrated on Figure 2, the compressive stress along the pre-stretched direction is reduced to $\sigma_E - \sigma_P$, where σ_P is the tensile stress due to the pre-stretch. However, the compressive stress normal to the pre-stretched direction maintains to be σ_E (Figure 2). Therefore, the creases and craters tend to align along the pre-stretched direction due to the lower compressive stress along that direction (Video S1 and Figure 1C). The aligned creases can further connect into parallel lines in the polymer layer (Video S2, and Figure 1C).

Now we quantitatively analyze the various patterns generated by DEL. A phase diagram for the patterns has been provided in Figure 1B. The transition of different patterns on the phase

Q. Wang, M. Tahir, Dr. J. Zang, Prof. X. Zhao
Department of Mechanical Engineering
and Materials Science
Soft Active Materials Laboratory
Duke University
Durham, NC, 27708, USA
E-mail: xz69@duke.edu



DOI: 10.1002/adma.201200272

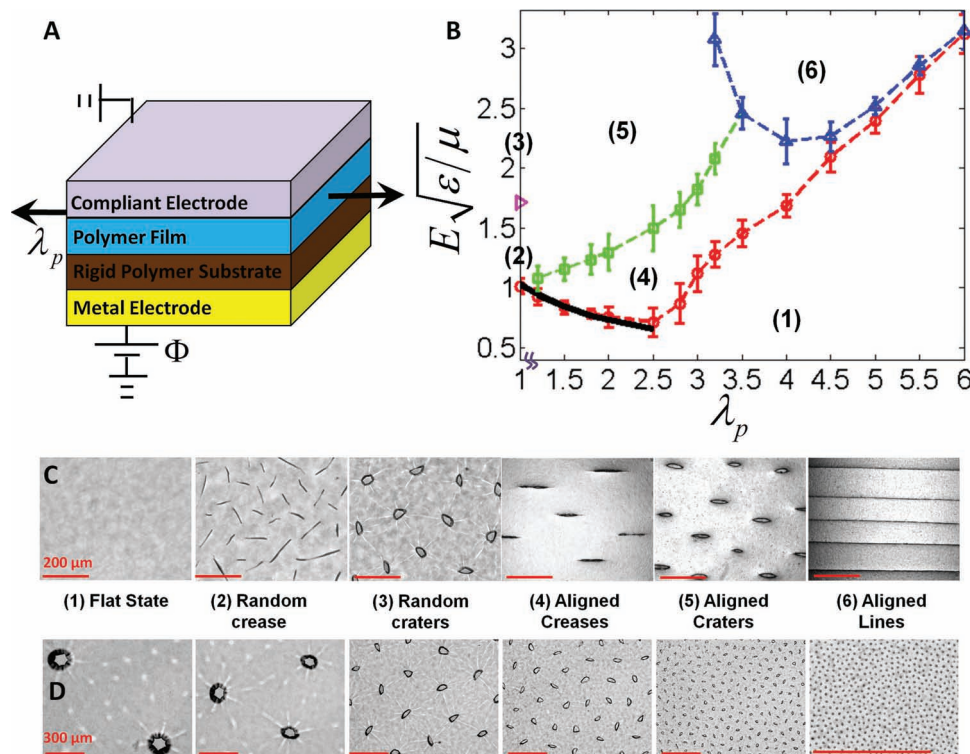


Figure 1. Pattern formation on polymer surfaces by dynamic electrostatic lithography (DEL). (A) Schematic illustration of the experimental set-up. (B) A phase diagram for the transition of patterns generated by DEL. The pattern transition is controlled by two parameters, the applied electric field E and the uniaxial pre-stretch ratio λ_p . The electric fields for the pattern transition were recorded as the critical electric fields, and plotted as the boundaries of the phase diagram. At least 5 experiments were conducted for each pre-stretch ratio to construct the error bar of the boundaries. (C) Optical microscope images of various patterns ranging from randomly-oriented creases and craters to aligned creases, craters and lines. The scale bars are 200 μm . (D) Optical microscope images of crater patterns with various wavelengths ranging from millimeter to micrometer. The scale bars are 300 μm .

diagram is controlled by two parameters, i.e. the applied electric field E and the uniaxial pre-stretch ratio λ_p . The applied field can be calculated as $E = \Phi / (h + H_s \epsilon / \epsilon_s)$, where Φ is the applied voltage, h and H_s the thicknesses of the pre-stretched polymer layer and the substrate, and ϵ and ϵ_s the dielectric constants of the polymer and the substrate. The pre-stretch ratio λ_p is given by the length of the pre-stretched layer over its undeformed length as shown in **Figure 3**. When a pattern becomes energetically favorable under a combination of E and λ_p , that pattern

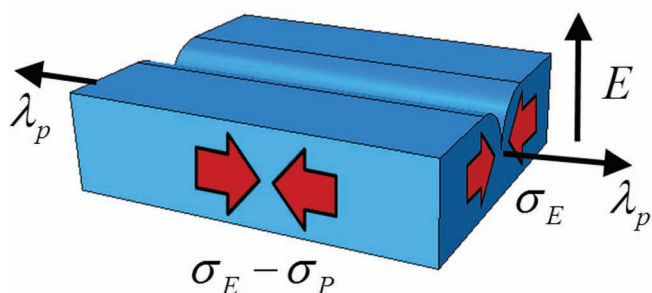


Figure 2. Schematic illustration of the stress in a uniaxially pre-stretched polymer layer under an electric field. The creases, craters and lines tend to align along the pre-stretched direction.

sets in the polymer layer. The potential energy of the polymer layer can be expressed as

$$\Pi = \int W(\lambda_1, \lambda_2, \lambda_3, \mathbf{E}) dV - \int \Phi \omega dA \quad (1)$$

where W is the free energy density of the polymer, and ω the surface charge density on the polymer. The free energy density

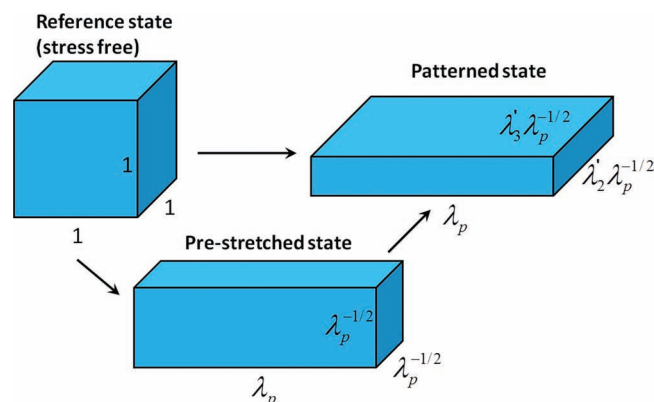


Figure 3. Schematic illustration of the principal stretches in a polymer layer at the reference, pre-stretched, and patterned states.

W is a function of the principal stretch λ_i and the electric field in the polymer E . The surface energy of the polymer layer is negligible in the current study.^[24,25] Because λ_i and E are generally inhomogeneous in patterned polymer layers, Equation (1) usually needs to be calculated with numerical models such as finite-element models.^[24,25,30]

Since the initiation of patterns (i.e. transition from flat to patterned states) is of particular importance to DEL, we will focus on calculating the critical electric field for the initiation of creases and lines on the phase diagram of Figure 1B. The polymer layer used in the current study (i.e. silicone elastomer) is taken to be an incompressible neo-Hookean ideal dielectric.^[24] When the polymer layer is pre-stretched by λ_p in one direction, the stretches in the other two directions are $\lambda^{-1/2}_p$ due to incompressibility of the polymer. Thus, the potential energy in a region of the polymer layer in the pre-stretched (flat) state can be expressed as

$$\Pi_{flat} = \frac{1}{2}\mu(\lambda_p^2 + 2\lambda_p^{-1} - 3)V - \frac{1}{2}\epsilon E^2 V \quad (2)$$

where μ is the shear modulus of the polymer, and V the volume of the region. The first term in Equation (2) gives the elastic energy of the polymer and the second term the electrostatic potential energy. Now let's consider the same region with a crease or line developed at a critical electric field, as illustrated on Figure 2. We can regard the pre-stretched state as another reference state, and express the stretches in the patterned state measured with respect to the pre-stretched state as λ'_1 , λ'_2 and λ'_3 as shown on Figure 3.^[30] Therefore, the principle stretches at the patterned state can be expressed as $\lambda_1 = \lambda'_1\lambda_p$, $\lambda_2 = \lambda'_2/\sqrt{\lambda_p}$, and $\lambda_3 = \lambda'_3/\sqrt{\lambda_p}$. Further assuming plane-strain condition^[24,25] for the patterned state as shown on Figures 2 and 3, we have $\lambda'_1 = 1$. Therefore, the potential energy in the region of the patterned state can be calculated as^[24,25]

$$\Pi_{pattern} = \int \frac{1}{2}\mu(\lambda_p^2 + \lambda'^2_2\lambda_p^{-1} + \lambda'^2_3\lambda_p^{-1} - 3)dV - \int \frac{1}{2}\epsilon|E|^2 dV \quad (3)$$

Based on Equations (2) and (3), the potential energy difference between the patterned and flat states can be calculated as

$$\Pi_{pattern} - \Pi_{flat} = \int \frac{\mu}{2\lambda_p}(\lambda'^2_2 + \lambda'^2_3 - 2)dV - \int \frac{1}{2}\epsilon(|E|^2 - E^2)dV \quad (4)$$

When the applied electric field E is 0, it is obvious that the flat state is energetically favorable as Equation (4) is positive. When E increases to a critical value, Equation (4) becomes 0 so that the creases or lines set in the polymer layer. Because μ , λ_p , and ϵ are constants in Equation (4), the electric fields can be rescaled by $\sqrt{\mu/(\epsilon\lambda_p)}$. Considering previous results,^[24] we can express the critical field for the initiation of patterns in uniaxially pre-stretched polymer layers as

$$E_c = Z\sqrt{\frac{\mu}{\lambda_p\epsilon}} \quad (5)$$

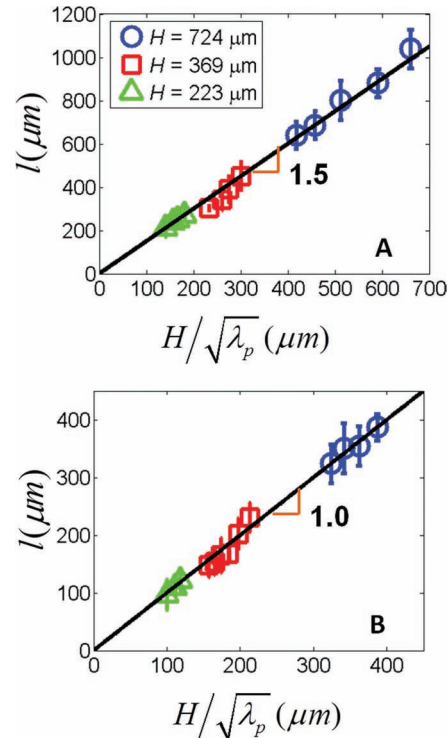


Figure 4. The wavelengths of aligned creases and craters (A) and aligned lines (B) are linearly proportional to the thicknesses of the pre-stretched polymer layers.

where Z is a non-dimensional constant which has been calculated to be 1.03 using finite-element models.^[24] From Equation (5), we can see that the uniaxial pre-stretch will decrease the critical electric field for the initiation of patterns. The theoretical prediction of Equation (5) has been plotted on Figure 1B. It can be seen that the theoretical prediction matches very well with experimental data when $\lambda_p \leq 2.5$. However, the experimental results show that the uniaxial pre-stretch increases the critical electric field when $\lambda_p > 2.5$. This is because the silicone rubber stiffens when $\lambda_p > 2.5$, ceasing to follow the neo-Hookean model (see Figure S2). The stiffening requires a higher electric field to deform the polymer layer,^[25] and thus increases the critical electric field E_c .

Next we discuss the wavelengths of patterns generated by DEL. The wavelengths can be tuned from millimeter to micrometer as shown qualitatively on Figure 1D and quantitatively on Figure 4. The tunable wavelength of DEL provides a broad range of feature sizes which are of critical importance to the applications of DEL in various technologies.^[1,2,3-7] Two parameters control the wavelengths of DEL patterns, i.e. the unstretched polymer thickness H and the uniaxial pre-stretch λ_p . Since the length scale for the interaction of two neighbor features (e.g. two creases, two craters or two lines) is the thickness of the film at the pre-stretched state, the wavelength of patterns can be expressed as

$$l = K\frac{H}{\sqrt{\lambda_p}} \quad (6)$$

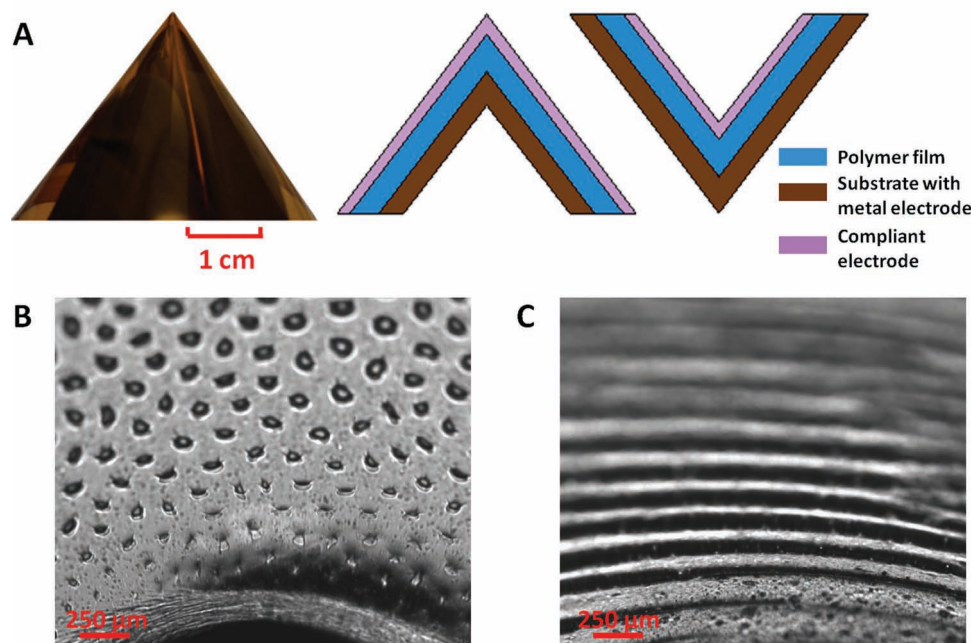


Figure 5. Pattern formation by DEL on large-area curved surfaces. (A) A cone-shape surface was produced by folding a polymer-substrate bilayer (See Figure S3 for experimental details). The polymer film can be on either the inner or outer surface of the cone. On the curved surface, randomly-oriented craters were formed in the polymer film without pre-stretch (B), and concentric circles were generated in the film with pre-stretch $\lambda_p = 5$ (C).

where l is the wavelength of the pattern, and K a non-dimensional constant. The prediction of Equation (6) has been validated by patterns of random creases and craters^[24]. Figure 4 further gives experimentally measured wavelengths of aligned creases, craters and lines on polymer layers with various values of H and λ_p . From Figure 4, it is evident that the theoretical prediction of Equation (6) matches consistently with the experimental results. In addition, Figure 4 gives that the parameter K in Equation (6) is ~ 1.5 for aligned creases and craters and ~ 1.0 for aligned lines.

Next we demonstrate the capability of DEL in generating various patterns on large-area and curved polymer surfaces. As illustrated in Figure 5A, a polymer layer is bonded on the inner or outer surface of a substrate of a cone shape (see Figure S3 for experimental details). The size of the cone is around 4 cm, and the radius of curvature of the polymer surface on the cone varies from a few micrometers to centimeters. If the polymer layer is not pre-stretched (i.e. $\lambda_p = 1$), random creases and craters can develop on the curved polymer surface under applied voltages (Figure 5B). If pre-stretched (e.g. $\lambda_p = 5$), the aligned lines arrange into concentric circles with well-defined distance on the polymer surfaces (Figure 5C).

In summary, we invent a new technology named *dynamic electrostatic lithography*, which is capable of dynamically generating patterns with various shapes and sizes on large-area curved polymer surfaces. The morphology of the patterns is controlled by the applied electric field and the pre-stretch in the polymer, and the wavelength is governed by the thickness of the pre-stretched polymer layer. A theory has been developed to calculate the critical electric fields for pattern transition and to predict the wavelengths of the patterns. The theoretical predictions match consistently with experimental results. A general

phase diagram is further constructed to characterize the transition between various patterns generated by DEL. The theory and the phase diagram will provide quantitative guidelines for future applications of DEL in various technologies.

Experimental Section

Silicon elastomer Ecoflex 00-10 (Smooth-on, USA) with volume ratio of two parts 0.2:1, was spin-coated on a glass slide covered by Scotch tape (3M, USA), and cured at room temperature for 12 hours. The thicknesses of the films were measured by Dektak 150 Stylus Profiler (Bruker AXS, USA), and the shear modulus of the Ecoflex film was measured by uniaxial tensile tests (TA instruments, USA). The uniaxially pre-stretched film of Ecoflex was adhered to a rigid polymer film, Kapton (Dupont, USA), which was bounded on a metal electrode. The top surface of the Ecoflex film was immersed in a transparent conformal electrode (e.g. 20 wt% NaCl solution) to observe the surface of the film. A voltage was applied between the two electrodes by a high voltage supply (Matsusada, Japan) with a ramping rate of 10 V/s. Images and videos of pattern formation on the polymer surface were recorded by a camera mounted on an optical microscope (Nikon, Japan). The electric voltages for the pattern transition were recorded as the critical voltages Φ_c and the critical electric fields were calculated by $E_c = \Phi_c / (h + H_s \epsilon / \epsilon_s)$, where h is the thickness of the pre-stretched Ecoflex film, $H_s = 125 \mu\text{m}$ is the thickness of the substrate, $\epsilon = 2.5\epsilon_0$ and $\epsilon_s = 3.5\epsilon_0$ are the dielectric constants of Ecoflex and Kapton respectively, and $\epsilon_0 = 8.85 \times 10^{-12} \text{ F m}^{-1}$ is the permittivity of vacuum. The wavelengths of the patterns were measured as average center-to-center distances of the neighbor features in the microscope image.

Supporting Information

Supporting Information is available from the Wiley Online Library or from the author.

Acknowledgements

The research is supported by the NSF's Research Triangle MRSEC (DMR-1121107). M.T. thanks the support from Lord Foundation. X.Z thanks the support from Haythornthwaite Research Initiation Grant.

Received: January 19, 2012

Published online: March 15, 2012

- [1] a) Y. N. Xia, J. A. Rogers, K. E. Paul, G. M. Whitesides, *Chem. Rev.* **1999**, *99*, 1823; b) G. M. Wallraff, W. D. Hinsberg, *Chem. Rev.* **1999**, *99*, 1801.
- [2] a) E. Schaffer, T. Thurn-Albrecht, T. P. Russell, U. Steiner, *Nature* **2000**, *403*, 874; b) M. D. Morariu, N. E. Voicu, E. Schaffer, Z. Q. Lin, T. P. Russell, U. Steiner, *Nat. Mater.* **2003**, *2*, 48.
- [3] T. Shimoda, K. Morii, S. Seki, H. Kiguchi, *MRS Bull.* **2003**, *28*, 821.
- [4] S. F. Lyuksyutov, R. A. Vaia, P. B. Paramonov, S. Juhl, L. Waterhouse, R. M. Ralich, G. Sigalov, E. Sancaktar, *Nat. Mater.* **2003**, *2*, 468.
- [5] N. E. Voicu, S. Ludwigs, U. Steiner, *Adv. Mater.* **2008**, *20*, 3022.
- [6] S. K. Sia, G. M. Whitesides, *Electrophoresis* **2003**, *24*, 3563.
- [7] S. J. Hollister, *Nat. Mater.* **2005**, *4*, 518.
- [8] a) S. Harkema, U. Steiner, *Adv. Funct. Mater.* **2005**, *15*, 2016; N. Arun, A. Sharma, V. B. Shenoy, K. S. Narayan, *Adv. Mater.* **2006**, *18*, 660; b) N. Wu, W. B. Russel, *Nano Today* **2009**, *4*, 180.
- [9] D. Salac, W. Lu, C. W. Wang, A. M. Sastry, *Appl. Phys. Lett.* **2004**, *85*, 1161.
- [10] N. Arun, A. Sharma, P. S. G. Pattader, I. Banerjee, H. M. Dixit, K. S. Narayan, *Phys. Rev. Lett.* **2009**, *102*, 254502.
- [11] J. Kim, J. Yoon, R. C. Hayward, *Nat. Mater.* **2010**, *9*, 159.
- [12] T. L. Sun, G. J. Wang, L. Feng, B. Q. Liu, Y. M. Ma, L. Jiang, D. B. Zhu, *Angew. Chem. Int. Ed.* **2004**, *43*, 357.
- [13] a) H. J. Gao, H. M. Yao, *Proc. Natl. Acad. Sci. USA* **2004**, *101*, 7851; b) E. P. Chan, E. J. Smith, R. C. Hayward, A. J. Crosby, *Adv. Mater.* **2008**, *20*, 711.
- [14] J. L. Wilbur, R. J. Jackman, G. M. Whitesides, E. L. Cheung, L. K. Lee, M. G. Prentiss, *Chem. Mater.* **1996**, *8*, 1380.
- [15] X. H. Zhao, J. Kim, C. A. Cezar, N. Huebsch, K. Lee, K. Bouhadir, D. J. Mooney, *Proc. Natl. Acad. Sci. USA* **2011**, *108*, 67.
- [16] L. K. Ista, S. Mendez, G. P. Lopez, *Biofouling* **2009**, *26*, 111.
- [17] M. A. Meitl, Z.-T. Zhu, V. Kumar, K. J. Lee, X. Feng, Y. Y. Huang, I. Adesida, R. G. Nuzzo, J. A. Rogers, *Nat. Mater.* **2006**, *5*, 33.
- [18] R. Marcombe, S. Q. Cai, W. Hong, X. H. Zhao, Y. Lapusta, Z. G. Suo, *Soft Matter* **2010**, *6*, 784.
- [19] Z. B. Yu, W. Yuan, P. Brochu, B. Chen, Z. T. Liu, Q. B. Pei, *Appl. Phys. Lett.* **2009**, *95*.
- [20] Y. Zhang, E. A. Matsumoto, A. Peter, P.-C. Lin, R. D. Kamien, S. Yang, *Nano Lett.* **2008**, *8*, 1192.
- [21] M. Guvendiren, J. A. Burdick, S. Yang, *Soft Matter* **2010**, *6*, 5795.
- [22] A. Ghatak, M. K. Chaudhury, V. Shenoy, A. Sharma, *Phys. Rev. Lett.* **2000**, *85*, 4329.
- [23] S. Cai, K. Bertoldi, H. Wang, Z. Suo, *Soft Matter* **2010**, *6*, 5770.
- [24] Q. Wang, L. Zhang, X. Zhao, *Phys. Rev. Lett.* **2011**, *106*, 118301.
- [25] Q. M. Wang, M. Tahir, L. Zhang, X. H. Zhao, *Soft Matter* **2011**, *7*, 6583.
- [26] M. D. Dickey, R. C. Chiechi, R. J. Larsen, E. A. Weiss, D. A. Weitz, G. M. Whitesides, *Adv. Funct. Mater.* **2008**, *18*, 1097.
- [27] A. R. Rathmell, S. M. Bergin, Y.-L. Hua, Z.-Y. Li, B. J. Wiley, *Adv. Mater.* **2010**, *22*, 3558.
- [28] W. Yuan, L. B. Hu, Z. B. Yu, T. L. Lam, J. Biggs, S. M. Ha, D. J. Xi, B. Chen, M. K. Senesky, G. Gruner, Q. B. Pei, *Adv. Mater.* **2008**, *20*, 621.
- [29] a) X. Zhao, W. Hong, Z. Suo, *Phys. Rev. B* **2007**, *76*, 134113; X. H. Zhao, Z. G. Suo, *Appl. Phys. Lett.* **2007**, *91*; b) C. Keplinger, M. Kaltenbrunner, N. Arnold, S. Bauer, *Proc. Natl. Acad. Sci. USA* **2010**, *107*, 4505.
- [30] W. Hong, X. Zhao, Z. Suo, *Appl. Phys. Lett.* **2009**, *95*, 111901.